

# Tetragonal and collapsed-tetragonal phases of $\text{CaFe}_2\text{As}_2$ – a view from angle-resolved photoemission and dynamical mean field theory

Ambroise van Roekeghem,<sup>1,2,\*</sup> Pierre Richard,<sup>1,3</sup> Xun Shi,<sup>1,4</sup> Shangfei Wu,<sup>1</sup> Lingkun Zeng,<sup>1</sup> Bayrammurad Saparov,<sup>5</sup> Yoshiyuki Ohtsubo,<sup>6</sup> Tian Qian,<sup>1</sup> Athena S. Sefat,<sup>5</sup> Silke Biermann,<sup>2,7,8</sup> and Hong Ding<sup>1,3</sup>

<sup>1</sup>*Beijing National Laboratory for Condensed Matter Physics, and Institute of Physics, Chinese Academy of Sciences, Beijing 100190, China*

<sup>2</sup>*Centre de Physique Théorique, Ecole Polytechnique, CNRS UMR 7644, 91128 Palaiseau, France*

<sup>3</sup>*Collaborative Innovation Center of Quantum Matter, Beijing, China*

<sup>4</sup>*Swiss Light Source, Paul Scherrer Institut, CH-5232 Villigen PSI, Switzerland*

<sup>5</sup>*Materials Science and Technology Division, Oak Ridge National Laboratory, Oak Ridge, Tennessee 37831-6114, USA*

<sup>6</sup>*Synchrotron SOLEIL, Saint-Aubin-BP 48, F-91192 Gif sur Yvette, France*

<sup>7</sup>*Collège de France, 11 place Marcelin Berthelot, 75005 Paris, France*

<sup>8</sup>*European Theoretical Synchrotron Facility, Europe*

We present a study of the tetragonal to collapsed-tetragonal transition of  $\text{CaFe}_2\text{As}_2$  using angle-resolved photoemission experiments and dynamical mean field theory-based electronic structure calculations. We observe that the collapsed-tetragonal phase exhibits reduced correlations and a higher coherence temperature due to the stronger Fe-As hybridization. Furthermore, a comparison of measured photoemission spectra and theoretical spectral functions shows that momentum-dependent corrections to the density functional band structure are essential for the description of low-energy quasiparticle dispersions. We introduce those using the recently proposed combined “Screened Exchange + Dynamical Mean Field Theory” scheme.

PACS numbers: 71.27.+a, 79.60.-i, 74.70.Xa, 71.45.Gm

## I. INTRODUCTION

$\text{CaFe}_2\text{As}_2$  at ambient pressure and temperature is in a paramagnetic tetragonal phase. When temperature is lowered under 170 K it develops a collinear antiferromagnetic order and becomes orthorhombic [1–3]. Under pressure, this orthorhombic phase can be suppressed and replaced by a non-magnetic collapsed-tetragonal phase in which the distance between two FeAs layers is strongly reduced due to the formation of covalent bonds between As atoms from two different layers. Superconductivity can also develop from this collapsed phase [4, 5]. Recently, it has been found that a quench of the annealing phase during crystal synthesis can produce samples presenting similar properties as  $\text{CaFe}_2\text{As}_2$  under pressure [6, 7]. At ambient temperature and pressure, they are in the tetragonal phase, and when temperature is lowered there is a transition into a collapsed-tetragonal phase, around 90 K in our samples [7]. There are also other ways to induce a collapse transition at ambient pressure, such as isovalent substitution of As by P [8], electron-doping by Rh at the Fe site [9] or electron doping by rare-earth on the Ca site [10]. However, while  $\text{CaFe}_2\text{As}_2$  in the collapsed-tetragonal phase can become superconductor under pressure [36] or with rare-earth doping [4, 10], it is not the case in these quenched crystals.

During the collapse, the  $c$  axis of the unit cell is strongly reduced by about 10%, while the  $a$  axis is enlarged by about 2%. This modification of the crystal structure is at the origin of a reorganization of the Fermi surface and electronic structure of the compound

[8, 9, 11–13], which has been studied within DFT [8, 14–16] and very recently within combined density functional dynamical mean field theory (“DFT+DMFT”) [17, 18]. In particular, it was found that the electronic correlations are reduced in the collapsed phase. Interestingly, the resistivity at the transition changes its low-energy behavior from  $\rho \propto T$  or  $\rho \propto T^{1.5}$  in the tetragonal phase to  $\rho \propto T^2$  – as in a good Fermi liquid – in the collapsed-tetragonal phase [7, 9, 19]. In rare-earth electron-doped  $\text{Ca}_{1-x}\text{RE}_x\text{Fe}_2\text{As}_2$ , this Fermi-liquid like resistivity is also observed at low temperature, independently of the stable phase – collapsed-tetragonal or non-collapsed-tetragonal as in  $\text{Ca}_{1-x}\text{La}_x\text{Fe}_2\text{As}_2$  [10]. Recent Nuclear Magnetic Resonance data further indicate a suppression of antiferromagnetic spin fluctuations in the collapsed-tetragonal phase [20]. Motivated by these intriguing results, we have performed DFT+DMFT calculations and ARPES experiments on the tetragonal and collapsed-tetragonal phase of  $\text{CaFe}_2\text{As}_2$ .

## II. THE COLLAPSE TRANSITION AS SEEN BY ARPES

We have performed angle-resolved photoemission measurements on samples grown by the self-flux method that are quenched from 960°C (corresponding to as-grown “p1” samples in [7]). Experiments were conducted at the CAS-SIOPEE beamline of SOLEIL synchrotron (France) and at the Institute of Physics, Chinese Academy of Sciences (China). Both systems are equipped with VG-Scienta R4000 electron analyzers. All samples were cleaved *in*

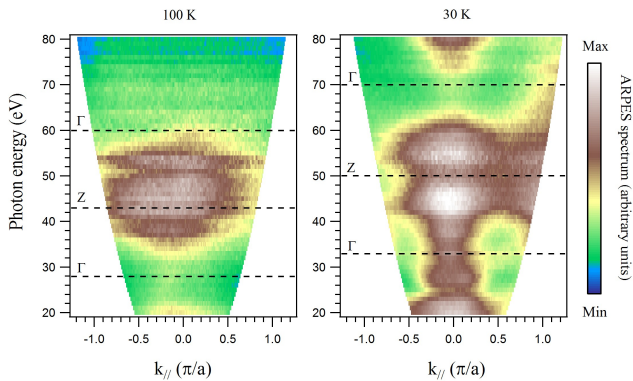


Figure 1: (Color online). Photon energy dependence of the ARPES spectra of  $\text{CaFe}_2\text{As}_2$  in the tetragonal ( $T = 100$  K) and collapsed-tetragonal ( $T = 30$  K) phases at the Fermi level around the  $\Gamma$  point.

*situ* at temperatures higher than 200 K and measured in a working vacuum between  $5 \times 10^{-10}$  and  $1 \times 10^{-9}$  torr at SOLEIL, and better than  $5 \times 10^{-11}$  torr at the Institute of Physics. The photon energy was varied from 20 to 80 eV in synchrotron while we used the He  $\text{I}\alpha$  line of an helium discharge lamp in the lab (21.218 eV). The angular resolution was better than  $0.5^\circ$  and the energy resolution better than 10 meV.

Samples were measured at 200 K, 100 K, 80 K and 30 K. The tetragonal to collapsed-tetragonal transition is shown to occur around 90 K by our magnetic susceptibility measurements, with a hysteresis smaller than 5 K, in agreement with [7]. Although we have performed the temperature-dependent measurements at the Institute of Physics, the Fermi surfaces obtained in SOLEIL are similar to those obtained in our laboratory, indicating that the measured samples are in the same phase.

Fig. 1 displays the photoemission spectra centered on the  $\Gamma$  point at the Fermi level for different spectra photon energies, in the collapsed-tetragonal and tetragonal phases. From the observed periodicity of the spectrum in the collapsed-tetragonal phase we find that the  $\Gamma$  point is located around 33 eV and 70 eV whereas a Z point is found around 50 eV. Using the sudden approximation and nearly free-electron model for the final state:  $k_\perp = \sqrt{2m(E_{kin} \cos^2 \theta + V_0)}/\hbar$  and the lattice parameters of Saparov *et al.* [7], we deduce an inner potential  $V_0$  of about 15 eV, which is consistent with other Fe-based superconductors [21]. This value of the inner potential also corresponds well to the data observed by Dhaka *et al.* [12]. In the tetragonal phase the data are less clear, but using the same value for  $V_0$  we estimate the  $\Gamma$  point to be around 28 eV and 60 eV and the Z point around 43 eV. This assumption is plausible at 28 eV, even though for higher photon energy there seems to be a slight discrepancy with the observed spectrum. This might be due to a modification of the inner potential since the surface

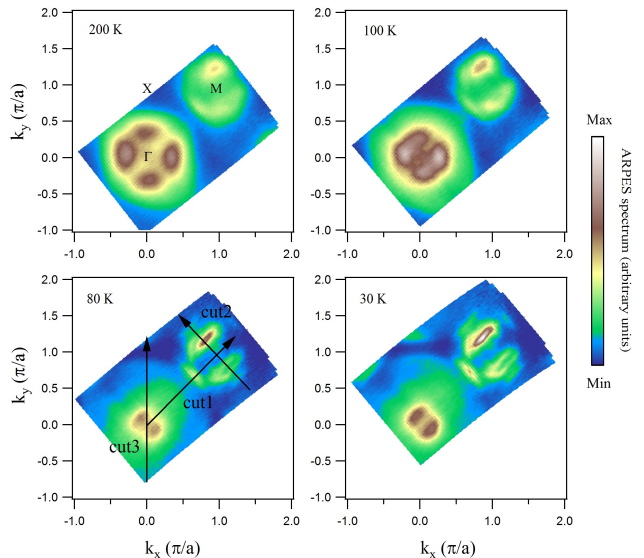


Figure 2: (Color online). Fermi surface mapping of  $\text{CaFe}_2\text{As}_2$  in the tetragonal ( $T > 90$  K) and collapsed-tetragonal ( $T < 90$  K) phases.

will probably be different in the tetragonal phase.

Fig. 2 shows the Fermi surface of our  $\text{CaFe}_2\text{As}_2$  sample in the tetragonal and collapsed-tetragonal phases recorded with a photon energy of 21.218 eV. We have lowered the temperature from 200 K to 30 K and finished the measurements less than 30 hours after the cleave, such that the aging of the sample was not important. Using the previously deduced inner potential, we find that for the collapsed-tetragonal phase the  $\Gamma$  point [37] has a  $k_z$  close to  $1.25 \pi/c'$  – with  $c' = c/2$  the distance between two FeAs layers, close to the Z point of coordinates  $(0, 0, \pi/c')$ .  $k_z$  then decreases when  $k_\parallel$  is increased, with a value of  $0.89 \pi/c'$  at the M point and  $1.01 \pi/c'$  at the X point. It is interesting to note that the point symmetric to  $\Gamma$  with respect to the X point would have for coordinates  $(2\pi/a, 0, 0.5\pi/c')$ , such that it would nearly correspond to the same high-symmetry point [38]. For the tetragonal phase, we find  $k_z = 1.6\pi/c'$  at the  $\Gamma$  point and  $k_z = 1.19\pi/c'$  at the M point.

For a more detailed analysis of the states forming the Fermi surface, we also present three different cuts. We first show the  $\Gamma$ -M direction for all temperatures (see Fig. 3 for the spectra and its curvature [22]). We also display a cut near the M point on the direction perpendicular to  $\Gamma$ -M (see Fig. 4 left panel) and another one along the  $\Gamma$ -X direction (Fig. 4 right panel), for the collapsed-tetragonal phase at 80 K only (similar results are obtained at 30 K). In the tetragonal phase, we can distinguish two hole-like bands forming circular hole pockets near the  $\Gamma$  point, although one may not cross the Fermi level. We also find two electron pockets around the M point. This is similar to what is found in many iron pnictides, and in particu-

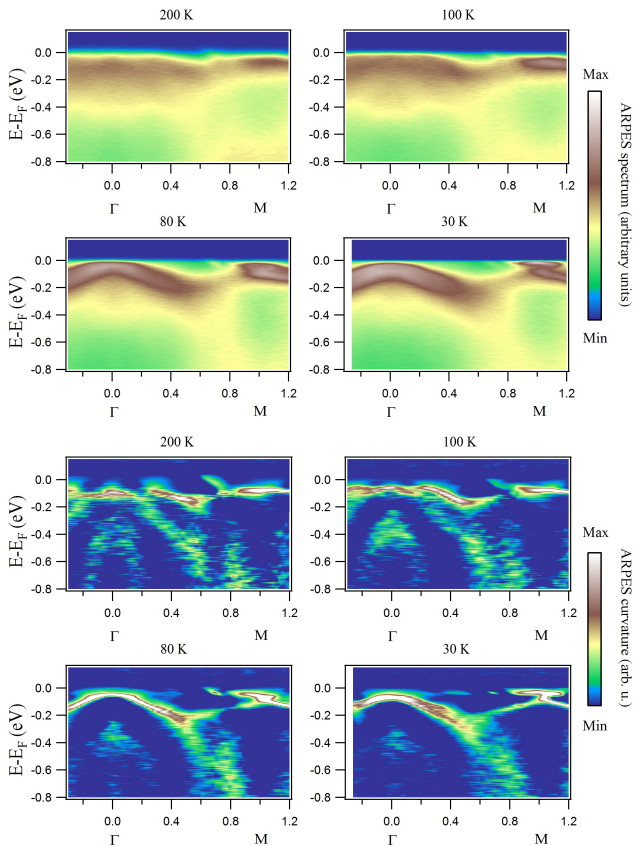


Figure 3: (Color online). ARPES spectra (top) and curvature (bottom) of  $\text{CaFe}_2\text{As}_2$  in the tetragonal ( $T > 90$  K) and collapsed-tetragonal ( $T < 90$  K) phases along cut 1 of Fig. 2.

lar in  $\text{BaFe}_2\text{As}_2$ . Below the transition temperature, the Fermi surface is reorganized. The circular hole pocket around the  $\Gamma$  point shrinks drastically – or even disappears – while a large square hole pocket develops. This shape of the hole-like bands is very characteristic of the collapsed structure and qualitatively different from what is seen in  $\text{BaFe}_2\text{As}_2$  [23]. This effect is due to a stronger three-dimensional character, as can be observed from the photon-energy dependent data of Fig. 1. Indeed, the  $k_z$  dispersion is enhanced by the strong As-As  $p_z$  interlayer hybridization in the collapsed phase. On the other hand, the electron pockets near M keep a similar size.

From the temperature-dependent photoemission spectra of Fig. 2, it is interesting to see how the features become better defined as temperature is lowered. Notably, there is a clear difference between spectra above (at 100 K) and below (at 80 K) the collapse transition. However, because the quasiparticle dispersions are also changed through this transition, and because overall the spectrum appears to be very sensitive to temperature, it is difficult to attribute this improvement to the transition only.

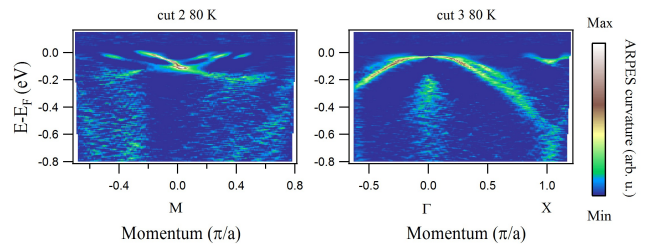


Figure 4: (Color online). Curvature of the ARPES spectra of  $\text{CaFe}_2\text{As}_2$  in the collapsed-tetragonal phase ( $T < 90$  K) along cut 2 (near the M point, left) and along cut 3 (right) of Fig. 2.

	$d_{z^2}$	$d_{x^2-y^2}$	$d_{xy}$	$d_{xz+yz}$
Tetragonal	1.43	1.37	1.64	1.57
collapsed-tetragonal	1.35	1.36	1.45	1.46

Table I: Mass renormalizations calculated from DFT+DMFT for the Fe-3d orbitals.

### III. DFT+DMFT CALCULATIONS

We now turn to a theoretical description of the spectral properties of  $\text{CaFe}_2\text{As}_2$ , using *first principles* dynamical mean field theory (DMFT) techniques. The first step are calculations based on the by now well-established DFT+DMFT method [24, 25]. We use the DFT+DMFT implementation of [26] within the Local Density Approximation (LDA) to the exchange-correlation functional, and Hubbard and Hund's interactions obtained from the constrained random phase approximation (cRPA) [27] in the implementation of Ref. [28]. The cRPA calculations yield  $F^0 = 2.5$  eV,  $F^2 = 6.0$  eV and  $F^4 = 4.5$  eV, corresponding to a Hund's rule coupling of  $J = 0.75$  eV.

Fig. 5 presents the superposition of bands extracted from DFT+DMFT calculations performed at 120 K with the ARPES spectrum along the  $\Gamma$ -M direction. We have taken into account the variation of  $k_z$  as indicated previously. Overall, the band renormalization is correctly described by the DFT+DMFT calculations. The theoretical quasi-particle renormalizations as extracted from a linearization around the Fermi energy of the imaginary part of the self-energy on the Matsubara axis are displayed in Table I. A caveat is however in order since the linear regime is really restricted to the first few Matsubara frequencies only, indicating that at the temperature of the calculation the system is at the border to an incoherent regime. Interestingly, on larger energy scales, at least in the tetragonal phase the self-energy can quite well be fit as a power law behavior  $\omega^\alpha$  with  $\alpha$  around 0.75. This is reminiscent to what was found in  $\text{BaFe}_2\text{As}_2$  in [29].

In agreement with Refs. [17, 18], we find the tetragonal phase to exhibit stronger electronic correlations than the collapsed phase. Within a given phase, we observe

stronger effects on the  $d_{xz+yz}$  and  $d_{xy}$  orbitals than on the  $d_{z^2}$  and  $d_{x^2-y^2}$  ones.

We can also see from the calculations that there may be three hole-like bands in total in the tetragonal phase but two are nearly degenerate near the  $\Gamma$  point. However, if we look at the precise details of the low-energy states, we can find several discrepancies. In the tetragonal phase at the Fermi level, one of the bands near the  $\Gamma$  point is not well described. It is not clear if this is due to possible surface effects, limitations of the calculations or other issues. On the other hand the electron pockets are well described. In the collapsed-tetragonal phase, the two hole-like bands near the  $\Gamma$  point appear to be very close to each other from photoemission measurements, as can be seen even more clearly on the 30 K data of Fig. 3 and along the  $\Gamma$ -X direction of Fig. 4. At the M point, two bands are responsible for the electron pockets, however the shape deviates from the experimental data due to upbending of one of the bands. On the other hand, we consider the agreement for the Fermi vector of the large hole pocket relatively satisfying since this band is very sensitive to the precise value of  $k_z$ . If we suppose that the ARPES spectrum reflects the bulk features of the collapsed-tetragonal phase, an important test for improved calculational schemes will be the correct prediction of the dispersion of the two hole-like bands near  $\Gamma$ , and of the interesting topology found near the M point in Fig. 4, which shows three bands crossing the Fermi level very close to each other – one of them being the large hole pocket. This last point is very specific to this compound in the iron pnictides family and due to the large  $k_z$  dispersion of the collapsed phase. We will present results beyond current DFT+DMFT techniques for  $\text{CaFe}_2\text{As}_2$  in section 5 below.

#### IV. INTERPLAY OF STRUCTURAL AND ELECTRONIC PROPERTIES WITHIN DFT+DMFT: INTERLAYER VERSUS INTRALAYER GEOMETRIES

The origin of the reduction of correlations in the collapsed-tetragonal phase compared to the tetragonal phase is challenging to understand since both Fe-As and As-As bindings are modified. Indeed, in the collapsed structure the As-As interlayer binding is much stronger, which should increase the three-dimensional character of the band structure dispersion. However, the transition has also another effect on the Fe-As binding since the  $c$  axis collapses so much that the As height to the Fe plane is reduced. The result is that the Fe-As distance is shortened, suggesting an enhancement of the hybridization between the As-4p and the Fe-3d orbitals – though the expansion of the  $a$  axis limits this enhancement.

To decouple these two effects we have performed DFT+DMFT calculations on two hypothetical “hybrid”

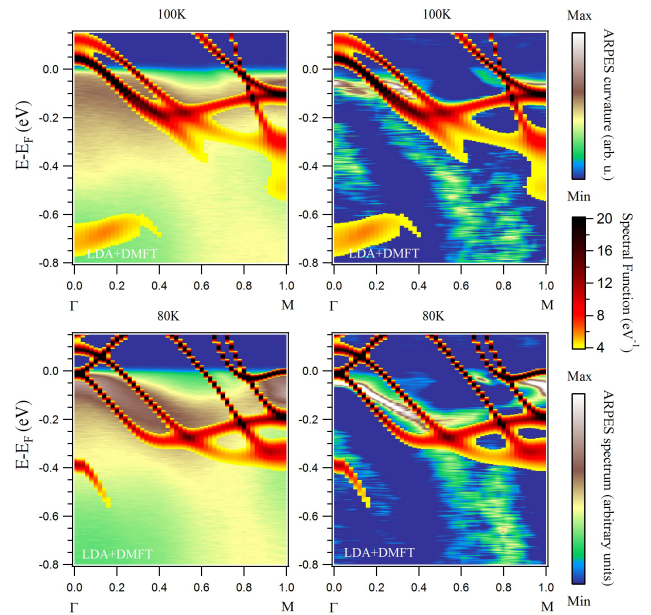


Figure 5: (Color online). Comparison of DFT+DMFT spectral functions with ARPES spectra of  $\text{CaFe}_2\text{As}_2$  in the tetragonal and collapsed-tetragonal phases. The parts of the spectral functions with value higher than  $4 \text{ eV}^{-1}$  are superimposed on the ARPES data of  $\text{CaFe}_2\text{As}_2$  in the tetragonal (100 K) and collapsed-tetragonal (80 K) phases along the  $\Gamma$ -M direction, represented using the (left) spectra or (right) curvature.

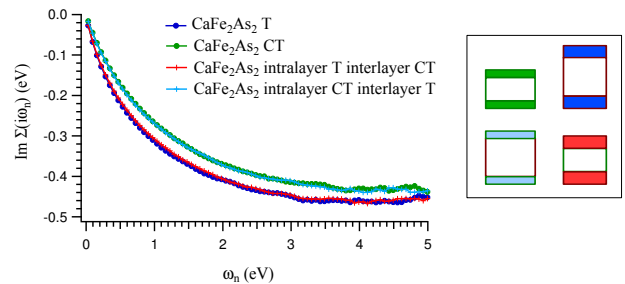


Figure 6: (Color online). Imaginary part of the self-energy in Matsubara frequencies of the  $d_{xy}$  orbital for  $\text{CaFe}_2\text{As}_2$  in the tetragonal structure (T), collapsed-tetragonal structure (CT) and in two hypothetical structures mixing the interlayer (i.e. As-As interlayer distance) and intralayer (i.e. intralayer Fe and As angles and distances) of the tetragonal and collapsed-tetragonal structures. The inset shows a schematic view of the different structures (colours correspond to the legend).

compounds. In the first one, we keep the same angle and distances between atoms within the FeAs layers as in the tetragonal phase, while the interlayer As-As distance is that of the collapsed-tetragonal phase. In the other one, we do the opposite: the layer is that of the collapsed-tetragonal phase and the interlayer distance is that of the tetragonal phase.

The imaginary part of the self-energy of the  $d_{xy}$  orbital in Matsubara frequencies is displayed in Fig. 6. The ef-

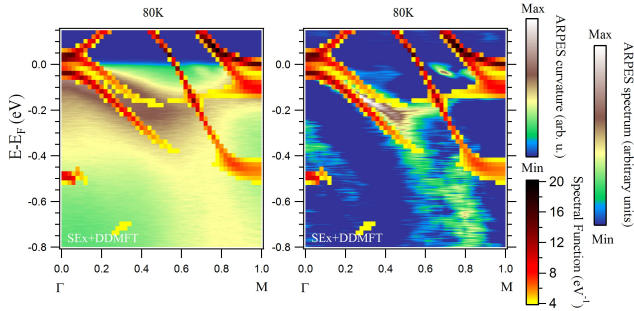


Figure 7: (Color online). Comparison of SEx+DDMFT spectral function with ARPES spectra of  $\text{CaFe}_2\text{As}_2$  in the collapsed-tetragonal phase. The parts of the spectral functions with value higher than  $4 \text{ eV}^{-1}$  are superimposed on the ARPES data of  $\text{CaFe}_2\text{As}_2$  along the  $\Gamma$ -M direction, represented using the (left) spectra or (right) curvature.

fect on the  $d_{xz} + d_{yz}$  orbital is similar, and since those orbitals have the highest density-of-states at the Fermi level we expect that they control the coherence properties of the compound [39]. We can first see that in the collapsed phase the imaginary part of the self-energy displays a more coherent behavior, which corresponds to the longer lifetime of quasiparticles displayed in Fig. 5. Furthermore, the shape of the self-energy of the hybrid compounds depends on the structure of the FeAs layer, while it is nearly insensitive to the interlayer As-As distance. Naturally, in reality those two effects are linked with each other, since the deformation of the FeAs layer is caused by the formation of As-As bonds that make the  $c$  axis collapse. Still, this numerical experiment indicates that within DFT+DMFT the improvement of coherence properties is not due to the interlayer As-As bonding but to the increase of the Fe-As hybridization within one single layer.

## V. BEYOND DFT+DMFT: RESULTS FROM SCREENED-EXCHANGE DYNAMICAL MEAN FIELD THEORY

Recently, some of us have proposed a new calculational scheme that goes beyond current DFT+DMFT techniques [30, 31]: the combination of a screened exchange Hamiltonian with “dynamical DMFT”, that is DMFT extended to dynamical Hubbard interactions [29, 32, 33] was shown to drastically improve upon the low-energy description of  $\text{BaCo}_2\text{As}_2$ . In this context, the apparent success of the standard DFT+DMFT scheme was shown to result from an error cancelation effect: a one-body Hamiltonian where the local exchange-correlation potential of DFT has been replaced by a non-local screened Fock term has in fact a wider band structure than the DFT one, but including dynamical screening effects at the level of the Hubbard interactions leads to addi-

tional renormalizations of the electronic states, as compared to usual DMFT. For this reason, the overall bandwidth of LDA+DMFT calculations and “Screened Exchange+Dynamical DMFT” (“SEx+DDMFT”) calculations are similar. The low-energy dispersions are however quite strongly improved by the introduction of the non-local screened exchange contribution.

In Fig. 7, we present the results of this SEx+DDMFT scheme, in the implementation of Ref. [30], applied to  $\text{CaFe}_2\text{As}_2$ . We use the frequency-dependent interactions as calculated in Ref. [34] and a value of  $\lambda = 1.7 a_0^{-1}$  for the screening wavelength which corresponds to the density-of-states at the Fermi level of the calculated result. As anticipated, due to the antagonistic effects of the non-local screened-exchange and of the high-frequency tail of the interactions, the overall renormalization of SEx+DDMFT is similar to the DFT+DMFT one. Still, the details of the quasiparticles dispersions at low energy are importantly modified. In the collapsed-tetragonal phase of  $\text{CaFe}_2\text{As}_2$ , the two bands observed near the  $\Gamma$  point are correctly described, in contrast to DFT+DMFT. The third large hole pocket is at variance with the calculations, but we stress that its precise Fermi vector is very sensitive on the value of  $k_z$ .

## VI. CONCLUSION

We have performed a study of the tetragonal and collapsed-tetragonal phases of  $\text{CaFe}_2\text{As}_2$  using ARPES and electronic structure calculations. Our results support the picture that within DMFT, the collapsed-tetragonal phase exhibits reduced correlations and higher coherence temperature due to the higher Fe-As hybridization, in agreement with other studies [17, 18]. However, we note that the reduction of correlations that we observe does not result in a dramatic change in the electronic self-energy that could explain by itself the behavior seen by resistivity measurements. This is confirmed by the ARPES results in the sense that the quasiparticle lifetimes away from the  $\Gamma$  point do not seem to be strongly impacted by the transition. Around the  $\Gamma$  point itself the electronic states found by photoemission appear more coherent but their dispersion has been largely reshaped by the collapse of the crystal. Furthermore, the unconventional transport behavior observed in experiments might not be the result of a change in electronic coherence alone. The reconstruction of the Fermi surface and of the low-energy electronic dispersion might induce geometric effects *via*, e.g. the Fermi surface nesting or dimensionality. Finally, at the temperature where the  $T -$  or  $T^{1.5}$  - behavior of the resistivity is observed, phonons likely also come into play.

## ACKNOWLEDGMENTS

We acknowledge useful discussions with Véronique Brouet and the coauthors of Ref. [30], in particular Thomas Ayrál, Michel Ferrero and Olivier Parcollet for support on the TRIQS toolkit [35]. We acknowledge SOLEIL for provision of synchrotron radiation facilities and we would like to thank François Bertran, Patrick Le Fèvre and Amina Taleb for assistance in using the beamline CASSIOPEE. This work was supported by the Cai Yuanpei program, IDRIS/GENCI Orsay under project 091393 and the European Research Council under project 617196. We also acknowledge grants from MOST (2010CB923000 and 2011CBA001000, 2011CBA00102, 2012CB821403) and NSFC (10974175, 11004232, 11034011/A0402, 11234014 and 11274362) from China. The work at Oak Ridge National Laboratory was primarily supported by the U. S. Department of Energy, Office of Science, Basic Energy Sciences, Materials Science and Engineering Division.

---

\* Electronic address: vanroeke@cphpt.polytechnique.fr

- [1] F. Ronning, T. Klimczuk, E. D. Bauer, H. Volz, and J. D. Thompson, *J. Phys.: Condens. Matter* **20**, 322201 (2008)
- [2] N. Ni, S. Nandi, A. Kreyssig, A. I. Goldman, E. D. Mun, S. L. Bud'ko, and P. C. Canfield, *Phys. Rev. B* **78**, 014523 (Jul 2008)
- [3] S. O. Diallo, V. P. Antropov, T. G. Perring, C. Broholm, J. J. Pulikkotil, N. Ni, S. L. Bud'ko, P. C. Canfield, A. Kreyssig, A. I. Goldman, and R. J. McQueeney, *Phys. Rev. Lett.* **102**, 187206 (May 2009)
- [4] M. S. Torikachvili, S. L. Bud'ko, N. Ni, and P. C. Canfield, *Phys. Rev. Lett.* **101**, 057006 (Jul 2008)
- [5] A. Kreyssig, M. A. Green, Y. Lee, G. D. Samolyuk, P. Zajdel, J. W. Lynn, S. L. Bud'ko, M. S. Torikachvili, N. Ni, S. Nandi, J. B. Leão, S. J. Poulton, D. N. Argyriou, B. N. Harmon, R. J. McQueeney, P. C. Canfield, and A. I. Goldman, *Phys. Rev. B* **78**, 184517 (Nov 2008)
- [6] S. Ran, S. L. Bud'ko, D. K. Pratt, A. Kreyssig, M. G. Kim, M. J. Kramer, D. H. Ryan, W. N. Rowan-Weetaluktuk, Y. Furukawa, B. Roy, A. I. Goldman, and P. C. Canfield, *Phys. Rev. B* **83**, 144517 (Apr 2011)
- [7] B. Sagarov, C. Cantoni, M. Pan, T. C. Hogan, W. Ratcliff II, S. D. Wilson, K. Fritsch, B. D. Gaulin, and A. S. Sefat, *Sci. Rep.* **4** (2014)
- [8] A. I. Coldea, C. M. J. Andrew, J. G. Analytis, R. D. McDonald, A. F. Bangura, J.-H. Chu, I. R. Fisher, and A. Carrington, *Phys. Rev. Lett.* **103**, 026404 (Jul 2009)
- [9] M. Danura, K. Kudo, Y. Oshiro, S. Araki, T. C. Kobayashi, and M. Nohara, *J. Phys. Soc. Jpn.* **80**, 103701 (2011)
- [10] S. R. Saha, N. P. Butch, T. Drye, J. Magill, S. Ziemak, K. Kirshenbaum, P. Y. Zavalij, J. W. Lynn, and J. Paglione, *Phys. Rev. B* **85**, 024525 (Jan 2012)
- [11] K. Tsubota, T. Wakita, H. Nagao, C. Hiramatsu, T. Ishiga, M. Sunagawa, K. Ono, H. Kumigashira, M. Danura, K. Kudo, M. Nohara, Y. Muraoka, and T. Yokoya, *J. Phys. Soc. Jpn.* **82**, 073705 (2013)
- [12] R. S. Dhaka, R. Jiang, S. Ran, S. L. Bud'ko, P. C. Canfield, B. N. Harmon, A. Kaminski, M. Tomić, R. Valentí, and Y. Lee, *Phys. Rev. B* **89**, 020511 (Jan 2014)
- [13] K. Gofryk, B. Sagarov, T. Durakiewicz, A. Chikina, S. Danzenbächer, D. V. Vyalikh, M. J. Graf, and A. S. Sefat, *Phys. Rev. Lett.* **112**, 186401 (May 2014)
- [14] T. Yildirim, *Phys. Rev. Lett.* **102**, 037003 (Jan 2009)
- [15] M. Tomić, R. Valentí, and H. O. Jeschke, *Phys. Rev. B* **85**, 094105 (Mar 2012)
- [16] R. S. Dhaka, Y. Lee, V. K. Anand, D. C. Johnston, B. N. Harmon, and A. Kaminski, *Phys. Rev. B* **87**, 214516 (2013)
- [17] S. Mandal, R. E. Cohen, and K. Haule, *Phys. Rev. B* **90**, 060501 (Aug 2014)
- [18] J. Diehl, S. Backes, D. Guterding, H. O. Jeschke, and R. Valentí, *Phys. Rev. B* **90**, 085110 (Aug 2014)
- [19] S. Kasahara, T. Shibauchi, K. Hashimoto, Y. Nakai, H. Ikeda, T. Terashima, and Y. Matsuda, *Phys. Rev. B* **83**, 060505 (Feb 2011)
- [20] Y. Furukawa, B. Roy, S. Ran, S. L. Bud'ko, and P. C. Canfield, *Phys. Rev. B* **89**, 121109 (Mar 2014)
- [21] P. Richard, T. Sato, K. Nakayama, T. Takahashi, and H. Ding, *Rep. Prog. Phys.* **74**, 124512 (2011)
- [22] P. Zhang, P. Richard, T. Qian, Y.-M. Xu, X. Dai, and H. Ding, *Rev. Sci. Instrum.* **82**, 043712 (2011)
- [23] T. Kondo, R. M. Fernandes, R. Khasanov, C. Liu, A. D. Palczewski, N. Ni, M. Shi, A. Bostwick, E. Rotenberg, J. Schmalian, S. L. Bud'ko, P. C. Canfield, and A. Kaminski, *Phys. Rev. B* **81**, 060507 (Feb 2010)
- [24] A. I. Lichtenstein and M. I. Katsnelson, *Phys. Rev. B* **57**, 6884 (Mar 1998)
- [25] V. I. Anisimov, A. Poteryaev, M. Korotin, A. Anokhin, and G. Kotliar, *J. Phys.: Condens. Matter* **9**, 943 (1997)
- [26] M. Aichhorn, L. Pourovskii, V. Vildosola, M. Ferrero, O. Parcollet, T. Miyake, A. Georges, and S. Biermann, *Phys. Rev. B* **80**, 085101 (Aug 2009)
- [27] F. Aryasetiawan, M. Imada, A. Georges, G. Kotliar, S. Biermann, and A. I. Lichtenstein, *Phys. Rev. B* **70**, 195104 (Nov 2004)
- [28] L. Vaugier, H. Jiang, and S. Biermann, *Phys. Rev. B* **86**, 165105 (2012)
- [29] P. Werner, M. Casula, T. Miyake, F. Aryasetiawan, A. J. Millis, and S. Biermann, *Nature Physics* **8**, 331 (2012)
- [30] A. van Roekeghem, T. Ayrál, J. M. Tomczak, M. Casula, N. Xu, H. Ding, M. Ferrero, O. Parcollet, H. Jiang, and S. Biermann, *Phys. Rev. Lett.* **113**, 266403 (2014)
- [31] A. van Roekeghem and S. Biermann, *EPL* **108**, 75003 (2014)
- [32] M. Casula, A. Rubtsov, and S. Biermann, *Phys. Rev. B* **85**, 035115 (Jan 2012)
- [33] L. Huang and Y. Wang, *EPL* **99**, 67003 (2012)
- [34] P. Seth, P. Hansmann, A. van Roekeghem, L. Vaugier, and S. Biermann, in preparation (2015)
- [35] M. Ferrero and O. Parcollet, "TRIQS: A toolbox for research on interacting quantum systems," (2011), <http://ipht.cea.fr/triqs>
- [36] Superconductivity can also occur in a non-collapsed phase, e.g. in  $\text{Ca}_{1-x}\text{La}_x\text{Fe}_2\text{As}_2$  [10] or for low-doping values in  $\text{CaFe}_2\text{As}_{2-x}\text{P}_x$  [19].
- [37] For simplicity, we name the points measured in Fig. 2 as their projection on the  $k_z = 0$  plane.
- [38] Indeed, the point Z with coordinates  $(0, 0, \pi/c')$  is equivalent to the point with coordinates  $(2\pi/a, 0, 0)$ .

[39] In contrast, there is no difference between the four structures for the  $d_{x^2-y^2}$  orbital and a much smaller one for

the  $d_{z^2}$  orbital.